Supplement of Aerosol Research, 4, 373–396, 2026
https://doi.org/10.5194/ar-4-373-2026-supplement


AEROSOL Research
Open Access

*Supplement of*

# Challenges in measuring sticky biogenic ice-nucleating macromolecules

**Joseph Robinson et al.**

*Correspondence to:* Joseph Robinson (eejr@leeds.ac.uk) and Benjamin J. Murray (b.j.murray@leeds.ac.uk)

## Data availability

The data associated with this publication is available at https://doi.org/10.5281/zenodo.19006498.

## S1 Handling Blanks

Throughout the experimental period, handling blanks were collected after the chamber has been flushed and/or cleaned and before the introduction of a new sample material. These blanks confirmed that the chamber background was sufficiently low to begin experiments and provided the background data used for background subtraction. Three handling blanks were collected during the Copper River dust and agricultural soil dust experiments, while one handling blank was collected for the pollen filtrate, Snomax filtrate, lichen filtrate, agricultural soil filtrate, and sea surface microlayer. No handling blank was collected before the dry Snomax experiments. The blanks were obtained on different days throughout the campaign following routine chamber cleaning. The blank spectra were assumed to be representative of the chamber background throughout the sampling period and were therefore used for background subtraction.

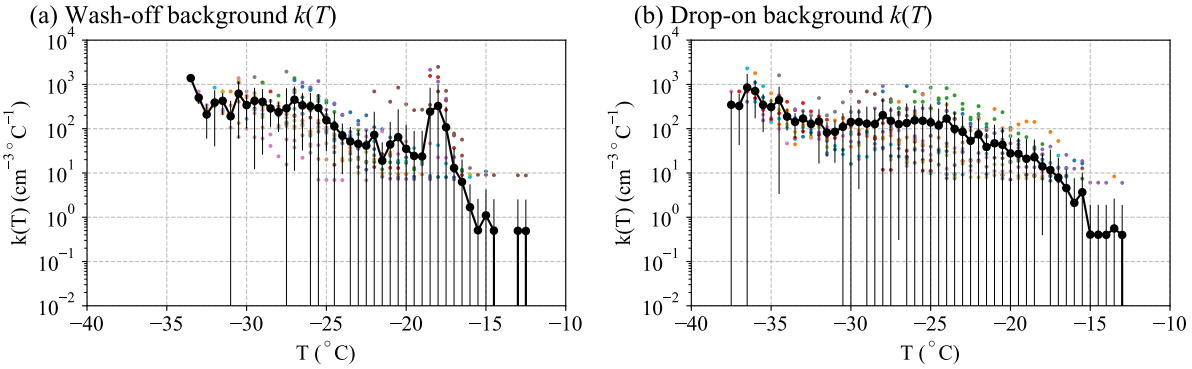


**Figure S1:** Differential freezing nucleus spectrum, $k(T)$, for the handling blanks for the (a) wash-off and (b) drop-on techniques. $k(T)$ was calculated for each handling blank and the average was found for each bin (including zeros) with the uncertainty being represented by the standard deviation.

Figure S1 shows the differential freezing nucleus spectrum, $k(T)$ data for the handling blank runs for the wash-off and drop-on techniques. For each handling blank, $k(T)$ was calculated in 0.5 °C temperature bins, and the mean and standard deviation were then calculated for each bin. These averaged backgrounds were used for all subsequent background subtraction steps for both filter techniques while the standard deviation represented the uncertainty of the background which ws then propagated through the calculation of the cumulative INP spectra.

## S2 Equivalence of Two Filter Samplers

To evaluate potential positional bias between the two filter sampling lines and verify that the chamber was well mixed by the fan, equivalence tests were conducted using agricultural soil dust and a cellulose sample that was ultimately not included in the study. PTFE filters were placed in both filter holders, and the collected samples were analysed using the drop-on technique. The resulting fraction frozen curves showed no systematic differences attributable to sampling location, with fraction frozen curves agreeing within approximately 1 °C (Figure S2). To further minimise any residual positional bias, the filter type assigned to each sampler was alternated throughout the experimental campaign.

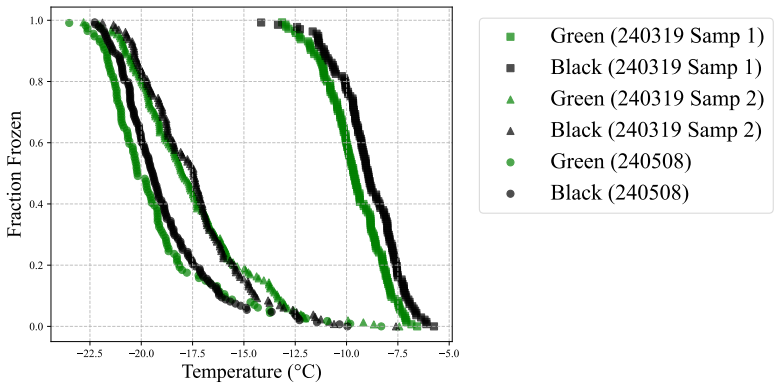


**Figure S2:** Fraction frozen curves from experiments conducted to asses the equivalence of the two filter sampling lines. PTFE filters were used in both sampling lines and analysed using the drop-on technique. The difference between the lines is within 1 °C, indicating no significant systematic bias is present.

# S3 Sampling Information and Individual Experiment Active Site Density Plots

The tables below (Table S1 to Table S8) summarise key parameters for each filter experiment, including sampling volume, average number concentration and surface area, their respective standard deviations ($\sigma$), and the peak diameter contributing to the surface area. Figure S4 and Figure S8 show the $\frac{dS}{d\log D_p}$ size distributions for the dry- and wet-dispersed experiments, respectively. Figure S5 to Figure S7 show $n_s(T)$ with associated uncertainties for the individual dry-dispersed experiments while Figure S9 to Figure S13 show $n_s(T)$ with associated error for wet-dispersed experiments.

## S3.1 Variability in Aerosol Size Distributions and Surface Area Concentrations

The particle size distributions shown in Figure S4 and Figure S8 exhibit some variability between experiments conducted using the same aerosol material. This variability was primarily associated with intentional changes in aerosol number concentration rather than uncontrolled changes in particle generation. We aimed to vary the aerosol loadings between experiments to extend the measurable range of $n_s(T)$ and to assess the performance of the wash-off and drop-on techniques over a range of total particle concentrations. Although these changes in loading produced modest differences in the measured size distributions, the overall distribution shape remained broadly consistent for a given material.

The temporal evolution of aerosol surface area concentration during each experiment is shown in Figure S3. For the dry-dispersed materials, aerosol surface area generally remained stable throughout the sampling period and, with the exception of Copper River Dust experiment 11, typically varied by less than an order of magnitude. Greater temporal variability was observed for the wet-dispersed experiments due to decreasing nebuliser reservoir volume and the repositioning of the nebuliser to restore aerosol concentrations. Nevertheless, the aerosol population remained sufficiently stable to allow for representative sampling throughout the experiments. As the dust tower and nebuliser were connected to the aerosol chamber by extended lengths of tubing, any particle losses due to settling or wall deposition would occur primarily upstream of the chamber. These losses were therefore inherently accounted for in the aerosol population measured by the APS/SMPS and sampled by both filter techniques.

The use of active site density assumes that ice-nucleating activity scales with particle surface

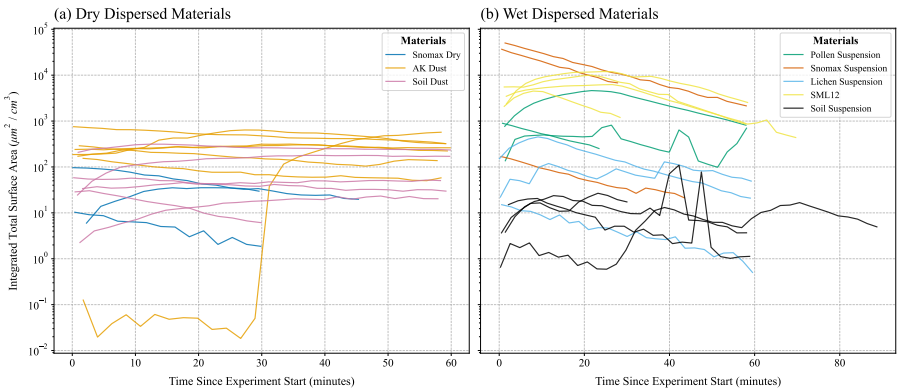


**Figure S3:** Time series of the integrated aerosol surface area concentration for all experiments. Dry-dispersed materials generally exhibited stable aerosol loadings through the sampling period, except for Copper River Dust experiment 11. Wet-dispersed materials tended to gradually decrease throughout the experiment with peaks associated with nebuliser repositioning to increase concentrations. The measurements demonstrate that aerosol populations remained broadly stable during sampling while allowing intentional variation in aerosol loading between experiments.

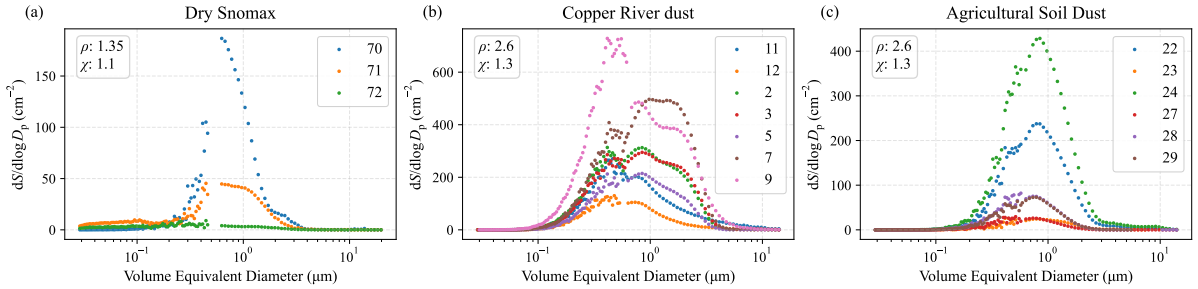


**Figure S4:** $\frac{\mathrm{d}S}{\mathrm{d}\log D_\mathrm{p}}$ size distributions for dry-dispersed samples from both the APS and SMPS data averaged over the experiment. The majority of the aerosol surface area is contributed to by particles near and above 1 $\mu$m, extending well into the supermicron range.

area and is therefore independent of particle size. While it is possible that particle composition, and thus $n_\mathrm{s}(T)$, may vary across particle size fractions, this effect is poorly constrained and is not explicitly accounted for within the $n_\mathrm{s}(T)$ framework. To minimise potential biases associated with this assumption, the dry- and wet-dispersion methods were selected to produce reproducible particle size distributions for each material and minimise variation in particle size between experiments.

Importantly, any variability in particle size distributions does not affect the comparison between the wash-off and drop-on techniques because both filter types collected particles simultaneously from the same aerosol population. Any temporal changes in aerosol concentration, surface area, or size distribution were experienced equally by both filter techniques, ensuring that the observed differences cannot be attributed to differences in the sampled aerosol.

## S3.2 Dry-Dispersed Samples

**Table S1:** Information about Dry Snomax Experiments.

| ID | Date | Volume (L) | Number Conc. ($cm^{-3}$) | Number Conc. $\sigma$ ($cm^{-3}$) | Surface Area ($\mu m^2 cm^{-3}$) | Surface Area $\sigma$ ($\mu m^2 cm^{-3}$) | Peak Diameter ($\mu m$) |
|---|---|---|---|---|---|---|---|
| 70 | 06/05/25 | 300 | 98.56 | 56.55 | 85.59 | 30.37 | 0.6 |
| 71 | 06/05/25 | 460 | 522.39 | 172.88 | 35.94 | 14.64 | 0.6 |
| 72 | 06/05/25 | 300 | 207.607 | 109.62 | 6.79 | 5.54 | 0.4 |

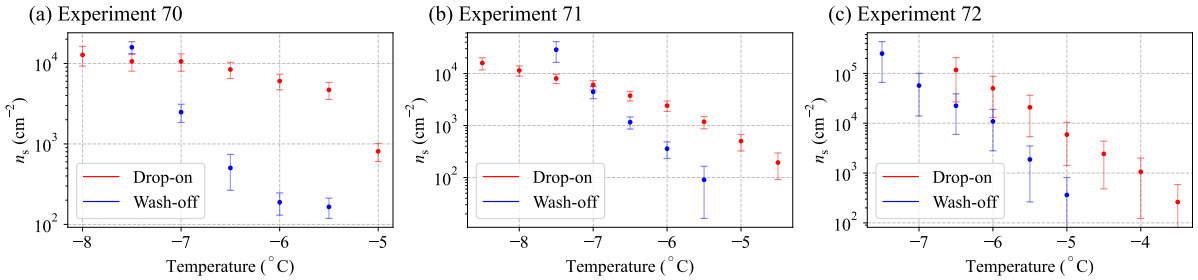


**Figure S5:** Active site density with error bars for all dry Snomax experiments.

**Table S2:** Information about Copper River dust Experiments.

| ID | Date | Volume (L) | Number Conc. ($cm^{-3}$) | Number Conc. $\sigma$ ($cm^{-3}$) | Surface Area ($\mu m^2 cm^{-3}$) | Surface Area $\sigma$ ($\mu m^2 cm^{-3}$) | Peak Diameter ($\mu m$) |
|---|---|---|---|---|---|---|---|
| 2 | 15/03/23 | 600 | 490.89 | 166.89 | 286.00 | 59.51 | 0.5 |
| 3 | 15/03/23 | 600 | 441.24 | 163.38 | 279.18 | 65.24 | 0.8 |
| 5 | 22/03/23 | 600 | 283.67 | 147.84 | 179.83 | 72.30 | 0.8 |
| 7 | 12/04/23 | 600 | 552.88 | 274.43 | 445.20 | 174.54 | 1 |
| 9 | 19/10/23 | 607.5 | 1097.00 | 333.20 | 566.18 | 170.04 | 0.5 |
| 11 | 30/10/23 | 600 | 405.76 | 510.06 | 194.92 | 247.43 | 0.4 |
| 12 | 30/10/23 | 600 | 210.89 | 129.30 | 89.72 | 47.82 | 0.5 |

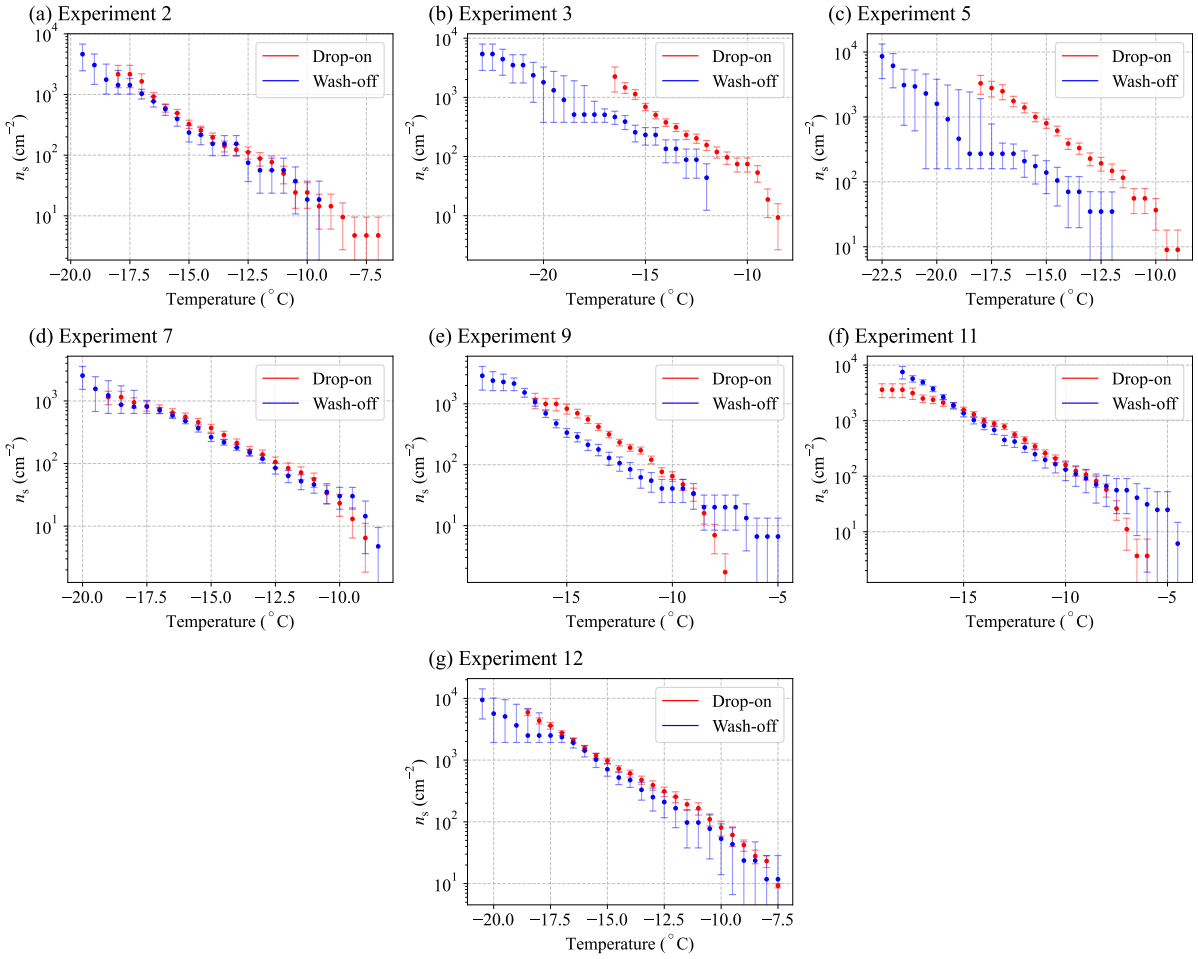


**Figure S6:** Active site density with error bars for all Copper River dust experiments.

**Table S3:** Information about Agricultural Soil Dust Experiments.

| ID | Date | Volume (L) | Number Conc. (cm$^{-3}$) | Number Conc. $\sigma$ (cm$^{-3}$) | Surface Area ($\mu$m$^2$cm$^{-3}$) | Surface Area $\sigma$ ($\mu$m$^2$cm$^{-3}$) | Peak Diameter ($\mu$m) |
|---|---|---|---|---|---|---|---|
| 22 | 20/03/24 | 610 | 170.41 | 104.66 | 151.53 | 63.91 | 0.8 |
| 23 | 21/03/24 | 320 | 22.20 | 28.14 | 16.81 | 14.29 | 0.7 |
| 24 | 22/03/24 | 600 | 282.95 | 123.33 | 271.83 | 63.80 | 0.8 |
| 27 | 02/05/24 | 600 | 28.66 | 34.16 | 16.72 | 13.87 | 0.7 |
| 28 | 02/05/24 | 600 | 75.67 | 56.01 | 47.96 | 20.30 | 0.7 |
| 29 | 03/05/24 | 600 | 62.83 | 50.17 | 42.54 | 19.83 | 0.8 |

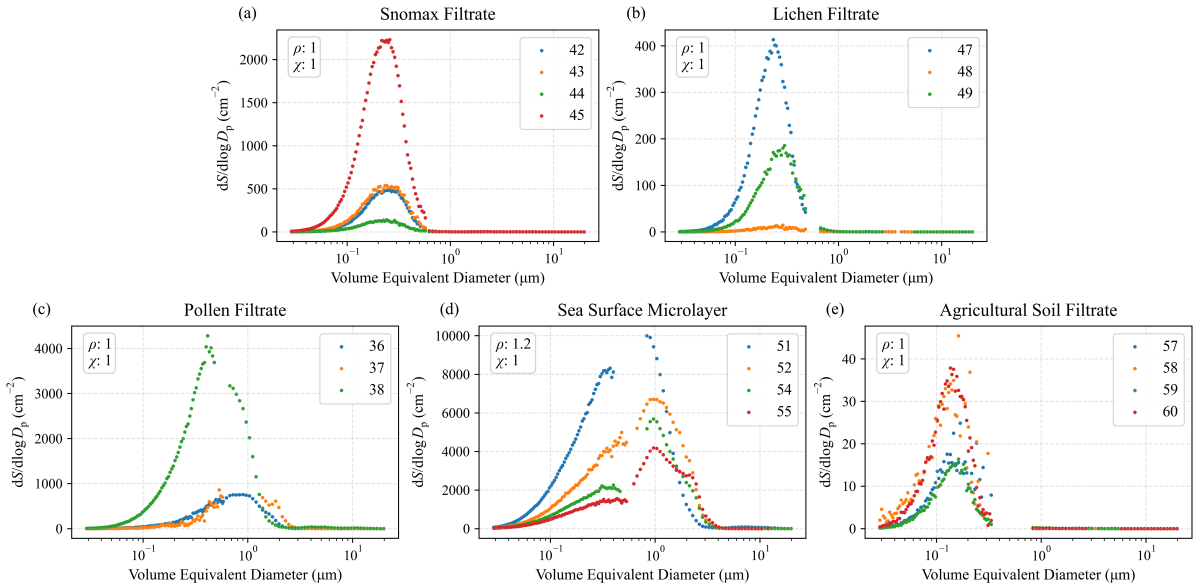


**Figure S8:** $\frac{\mathrm{d}S}{\mathrm{d}\log D_\mathrm{p}}$ size distributions for wet-dispersed samples from both the APS and SMPS data averaged over the experiment. The filtrate materials all peak in the accumulation mode. The sea surface microlayer was not filtered and contains some larger particles.

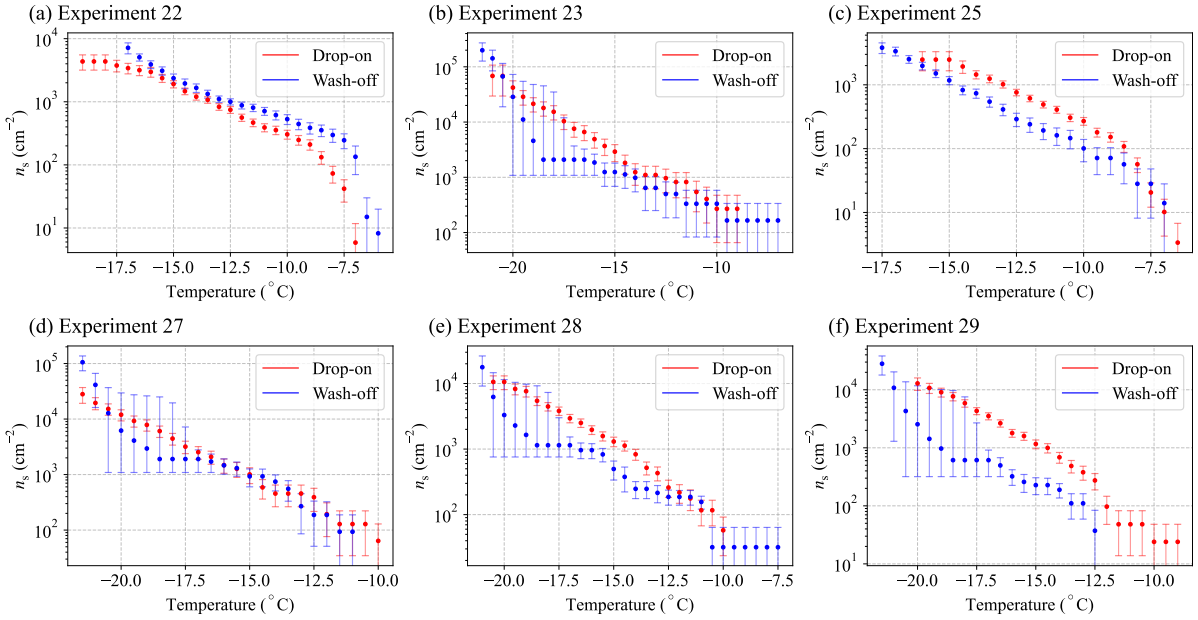


**Figure S7:** Active site density with error bars for all Agricultural Soil Dust experiments.

## S3.3 Wet-Dispersed Samples

**Table S4:** Information about Snomax Filtrate Experiments.

| ID | Date | Volume (L) | Number Conc. ($cm^{-3}$) | Number Conc. $\sigma$ ($cm^{-3}$) | Surface Area ($\mu m^2 cm^{-3}$) | Surface Area $\sigma$ ($\mu m^2 cm^{-3}$) | Peak Diameter ($\mu m$) |
|---|---|---|---|---|---|---|---|
| 40 | 17/05/24 | 600 | 894.90 | 1051.84 | 100.86 | 170.56 | 0.3 |
| 42 | 20/05/24 | 600 | 2611.33 | 2471.45 | 239.98 | 224.56 | 0.25 |
| 43 | 20/05/24 | 300 | 3198.33 | 1900.62 | 278.27 | 158.09 | 0.25 |
| 44 | 21/05/24 | 451.7 | 908.61 | 613.41 | 66.44 | 50.93 | 0.25 |
| 69[1] | 02/05/25 | N/A | N/A | N/A | N/A | N/A | N/A |

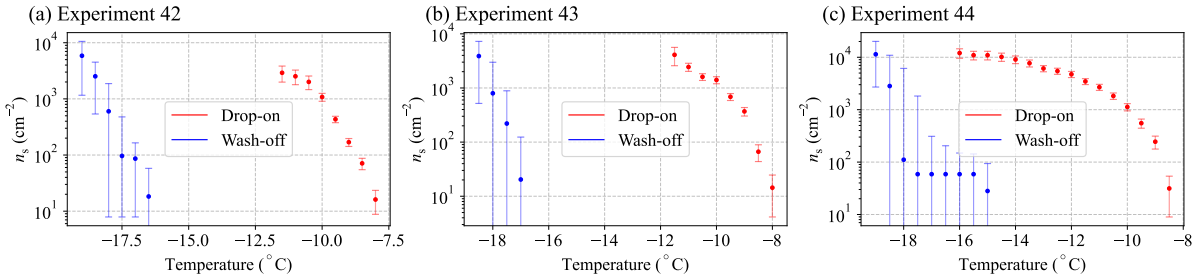


**Figure S9:** Active site density with error bars for all Snomax Filtrate experiments.

**Table S5:** Information about Lichen Filtrate Experiments.

| ID | Date | Volume (L) | Number Conc. ($cm^{-3}$) | Number Conc. $\sigma$ ($cm^{-3}$) | Surface Area ($\mu m^2 cm^{-3}$) | Surface Area $\sigma$ ($\mu m^2 cm^{-3}$) | Peak Diameter ($\mu m$) |
|---|---|---|---|---|---|---|---|
| 47 | 24/05/24 | 600 | 1807.33 | 1638.94 | 169.07 | 144.98 | 0.2 |
| 48 | 24/05/24 | 600 | 53.93 | 66.98 | 5.50 | 7.97 | 0.2 |
| 49 | 24/05/24 | 600 | 669.33 | 318.12 | 80.73 | 37.26 | 0.3 |

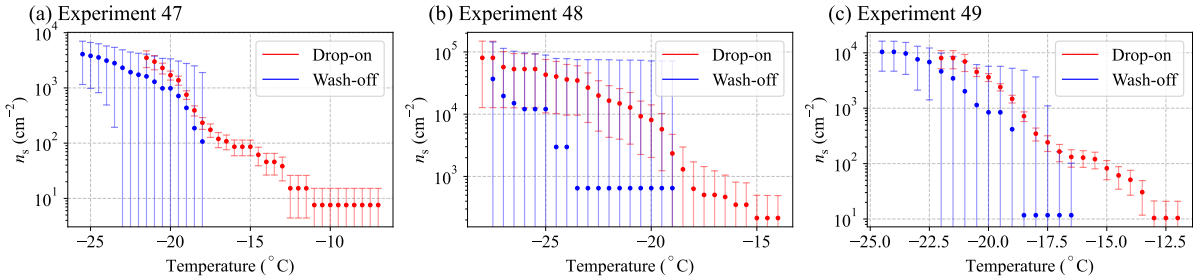


**Figure S10:** Active site density with error bars for all Lichen Filtrate experiments.

[1]PINE experiment only

**Table S6:** Information about Pollen Filtrate Experiments.

| ID | Date | Volume (L) | Number Conc. ($cm^{-3}$) | Number Conc. $\sigma$ ($cm^{-3}$) | Surface Area ($\mu m^2 cm^{-3}$) | Surface Area $\sigma$ ($\mu m^2 cm^{-3}$) | Peak Diameter ($\mu m$) |
|---|---|---|---|---|---|---|---|
| 36 | 14/05/24 | 250 | 1426.80 | 652.09 | 515.75 | 218.73 | 0.9 |
| 37 | 15/05/24 | 600 | 982.16 | 1569.88 | 540.53 | 600.25 | 0.9 |
| 38 | 15/05/24 | 600 | 11996.02 | 7238.38 | 2632.95 | 1380.14 | 0.4 |

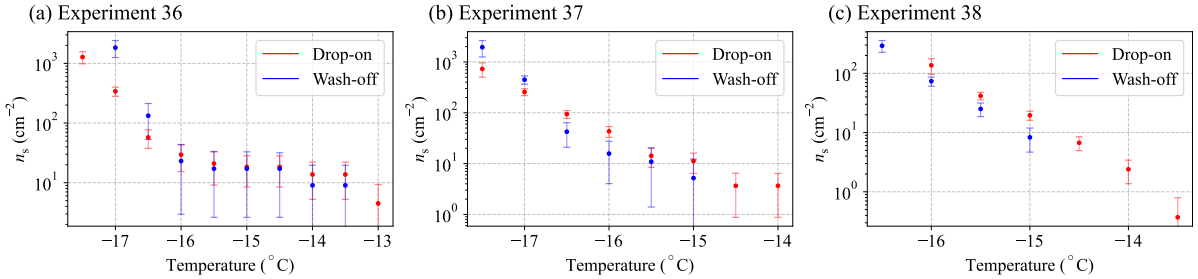


**Figure S11:** Active site density with error bars for all Pollen Filtrate experiments.

**Table S7:** Information about Sea Surface Microlayer Experiments.

| ID | Date | Volume (L) | Number Conc. ($cm^{-3}$) | Number Conc. $\sigma$ ($cm^{-3}$) | Surface Area ($\mu m^2 cm^{-3}$) | Surface Area $\sigma$ ($\mu m^2 cm^{-3}$) | Peak Diameter ($\mu m$) |
|---|---|---|---|---|---|---|---|
| 51 | 14/08/24 | 600 | 60876.39 | 32366.40 | 8956.88 | 3908.88 | 0.7 |
| 52 | 14/08/24 | 600 | 30485.23 | 19699.20 | 6001.87 | 3632.29 | 1 |
| 54 | 16/08/24 | 700 | 19304.24 | 11988.92 | 3987.13 | 2556.94 | 1 |
| 55 | 16/08/24 | 300 | 14287.07 | 5318.37 | 3174.25 | 1384.00 | 1 |

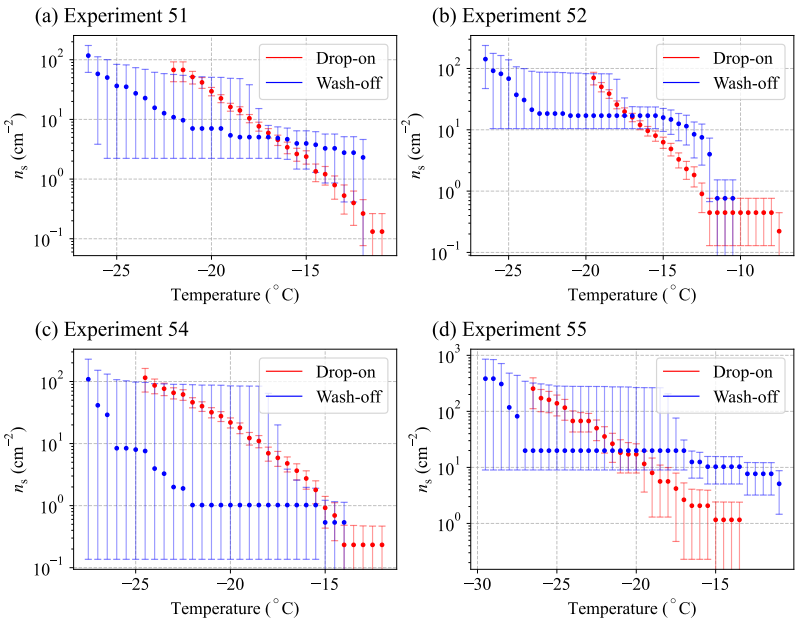


**Figure S12:** Active site density with error bars for all sea surface microlayer experiments.

**Table S8:** Information about Agricultural Soil Filtrate Experiments.

| ID | Date | Volume (L) | Number Conc. ($cm^{-3}$) | Number Conc. $\sigma$ ($cm^{-3}$) | Surface Area ($\mu m^2 cm^{-3}$) | Surface Area $\sigma$ ($\mu m^2 cm^{-3}$) | Peak Diameter ($\mu m$) |
|---|---|---|---|---|---|---|---|
| 57 | 20/08/24 | 600 | 219.26 | 279.02 | 10.66 | 21.06 | 0.15 |
| 58 | 21/08/24 | 600 | 607.92 | 1016.28 | 19.92 | 35.61 | 0.15 |
| 59 | 21/08/24 | 900 | 70.87 | 159.43 | 6.71 | 7.07 | 0.15 |
| 60 | 21/08/24 | 300 | 460.45 | 242.80 | 15.95 | 9.57 | 0.15 |

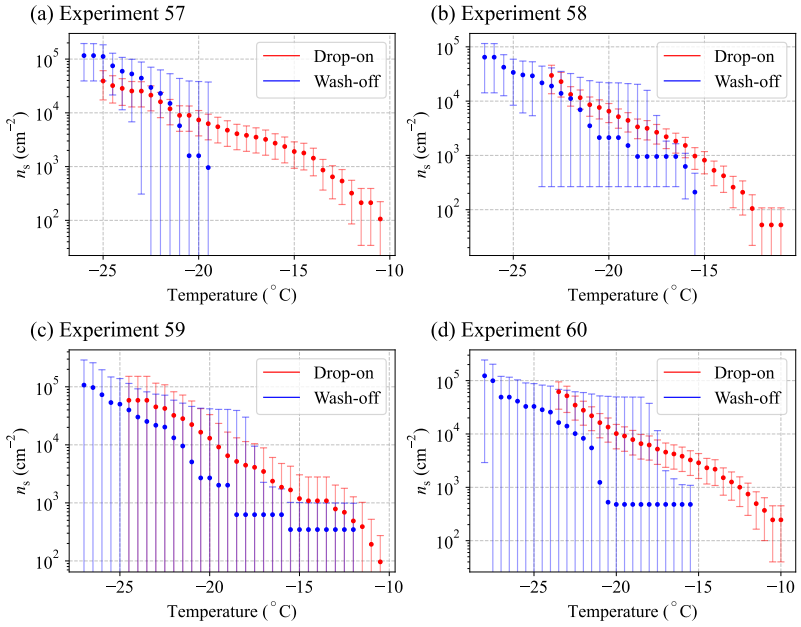


**Figure S13:** Active site density with error bars for all Soil Filtrate experiments.

## S4 Merging Particle Size Distributions

Particle size distributions were measured using a TSI Aerodynamic Particle Sizer (APS) and Scanning Mobility Particle Sizer (SMPS). The APS measures particles predominantly in the coarse mode (0.523 to 19.81 $\mu$m), while the SMPS measures primarily in the accumulation mode (0.0146 to 0.6854 $\mu$m), enabling measurements across three orders of magnitude. To merge the two datasets, both instrument diameters were converted to volume-equivalent diameters. The APS aerodynamic diameter was converted using the APS factor, $F_{APS}$, in Equation S1, while the SMPS electrostatic diameter was converted using the SMPS factor, $F_{SMPS}$, in Equation S2 [Möhler et al., 2008].

$$F_{APS} = \sqrt{\frac{\chi}{\rho}} \tag{S1}$$

$$F_{SMPS} = \frac{1}{\chi} \tag{S2}$$

Where $\chi$ is the dynamic shape factor, reflecting how spherical the particles are, and $\rho$ is the particle density (g $cm^{-3}$). $\chi$ and $\rho$ values used for each material are listed in Table S9. Some values were taken directly from the literature, where available. In other cases, $\chi$ and $\rho$ were

| Material | $\chi$ | $\rho$ | Source |
|---|---|---|---|
| Copper River Dust | 1.3 | 2.6 | Möhler et al. [2008] |
| Agricultural Soil Dust | 1.3 | 2.6 | Möhler et al. [2008] |
| Lichen Filtrate | 1 | 1 | Estimated (this study) |
| Agricultural Soil Filtrate | 1 | 1 | Estimated (this study) |
| Snomax Filtrate | 1 | 1 | Estimated (this study) |
| Sea Surface Microlayer | 1 | 1.2 | Estimated (this study) |
| Pollen Filtrate | 1 | 1 | Estimated (this study) |
| Dry Snomax | 1.1 | 1.35 | Wex et al. [2015] |

**Table S9:** Dynamic shape factor ($\chi$) and density ($\rho$) for each material in this study.

selected to produce reasonable continuity between the APS and SMPS size distributions while remaining consistent with expected physical properties of the aerosol particles. For example, aerosols generated from nebulised aqueous suspension were assumed to be approximately spherical and therefore assigned $\chi = 1$. For each experiment, the largest SMPS bins and smallest APS bins were removed as these bins are known to undercount. These processed volume median size distributions (Figure S4 and Figure S8) were then used to compute the total surface area (in Table S2 to Table S8). To determine the uncertainty in the total surface area, the error is propagated from the raw files. In the raw files, the number of particles detected in each bin is used to calculate the Poisson counting uncertainty. The percent error is then calculated and propagated through to the final total surface area value.

### S4.1 Sensitivity of $n_s(T)$ to $\chi$ and $\rho$

The dynamic shape factor ($\chi$) and particle density ($\rho$) are required to convert APS aerodynamic diameters and SMPS mobility diameters to volume-equivalent diameters prior to merging the size distributions. For some materials, values were available in the literature. For others, particularly the wet-dispersed samples, literature values were unavailable and physically reasonable estimates were adopted. To assess the sensitivity of the calculated aerosol surface area and active site density to these assumptions, the APS-SMPS merging procedure was repeated using different $\chi$ and $\rho$ values. The dynamic shape factor was increased by 20% relative to the baseline value used in the analysis, while density was increased and decreased by 20%. This range was selected to represent plausible uncertainty in the assumed particle properties and to assess the changes in the calculated $n_s(T)$ values.

Table S10 summarises the mean sensitivity for each sample material. Overall, $n_s(T)$ was generally more sensitive to changes in $\chi$ than $\rho$ because $\chi$ affects the conversion of both APS and SMPS diameters to volume-equivalent diameters, whereas $\rho$ only affects the APS diameter conversion. The largest changes were observed for wet-dispersed samples, whereas density variability only produced relatively small changes in $n_s(T)$ for most materials. For all materials, the mean differences between the wash-off and drop-on techniques exceeded the mean changes introduced by varying $\chi$ and $\rho$. Therefore uncertainty associated with the APS-SMPS merging parameters cannot explain the method-dependent differences reported in this study. In addition, both filter types were collected simultaneously from the same aerosol population and therefore share the same aerosol surface area estimate. This means that uncertainties arising from the merging of the APS and SMPS data affect both techniques equally and do not influence the relative comparison presented in this study. The conclusions regarding the differences between the wash-off and drop-on techniques are therefore robust to reasonable uncertainty in particle shape factor and density.

| Material | Mean —DO-WO— Difference (%) | Mean $\Delta n_s(T)$ ($\chi + 20\%$) (%) | Mean $\Delta n_s(T)$ ($\rho + 20\%$) (%) | Mean $\Delta n_s(T)$ ($\rho - 20\%$) (%) |
|---|---|---|---|---|
| Copper River Dust | 135.15 | -11.80 | 17.14 | -17.76 |
| Agricultural Soil Dust | 160.87 | -15.30 | 18.86 | -19.31 |
| Lichen Filtrate | 928.90 | 36.59 | 1.64 | -2.04 |
| Agricultural Soil Filtrate | 376.34 | 37.05 | 1.77 | -2.04 |
| Snomax Filtrate | 25925.26* | 42.40 | 0.23 | -0.44 |
| Sea Surface Microlayer | 449.34 | -5.21 | 13.46 | -15.09 |
| Pollen Filtrate | 51.88 | -6.41 | 13.94 | -15.65 |
| Dry Snomax | 921.58 | -8.13 | 15.67 | -16.51 |

**Table S10:** Mean percent difference in $n_s(T)$ between the wash-off and drop-on techniques and the corresponding sensitivity of calculated $n_s(T)$ to changes in dynamic shape factor ($\chi$) and particle density ($\rho$). Values are averaged across all experiment for each material type. *Only one Snomax filtrate experiment produced overlapping wash-off and drop-on datasets.

The largest sensitivity identified in this analysis was approximately 42% for the Snomax filtrate, where the corresponding mean difference between the wash-off and drop-on techniques exceeded $25,000\%$. The observed technique difference is therefore nearly three order of magnitude larger than the uncertainty introduced by the APS-SMPS merging parameters.

## S5 PINE Pressure Bins

In standard PINE data analysis, each expansion yields a single data point, where the temperature corresponds to the condition reached after expanding to a defined pressure. This produces a single cumulative ice-nucleating particle concentration at the lowest temperature of the expansion. This approach works well in cases where the INP concentration is very low, such as ambient aerosol, because only a small number of INPs are detected over the course of the expansion. However, in these laboratory experiments, the aerosol concentration is sufficiently high that a large number of particles activate to ice during a single expansion. Under these conditions, we can bin the data through an expansion to produce cumulative INP concentrations over a range of temperatures. We divided each expansion into five equal-sized pressure bins. For example, a 1000-750 hPa expansion yields the following bins: 1000-950 hPa, 950-900 hPa, 900-850 hPa, 850-800 hPa, and 800-750 hPa. The lowest temperature for each bin was estimated assuming adiabatic expansion, and INP concentration was calculated from the number of ice crystals detected within each bin and the volume of gas passing through the detection volume (at standard temperature and pressure).

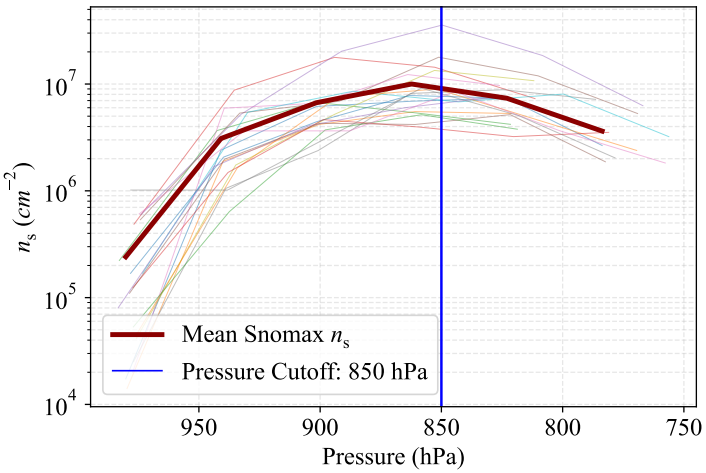


**Figure S14:** $n_s(T)$ vs pressure for all the dry Snomax experiments. The decrease in activity below 850 hPa is associated with the loss of ice crystals during the later stages of the expansion. This behaviour motivates the selection of 850 hPa as the lower pressure cutoff used throughout the PINE dataset.

By definition, $N_{INP}(T)$ is cumulative and therefore must increase (or stay constant) with decreasing temperature. However, when ice crystals grow during expansion, they can be lost from the chamber through sedimentation or impaction, leading to an apparent decrease in the measured cumulative INP concentration. In some experiments, we noted a decrease in $N_{INP}(T)$ in the lower temperature (pressure) bins, which is consistent with the loss of ice crystals from the chamber during the later stages of the expansion. To determine an appropriate lower pressure cutoff, we analysed the dry Snomax experiments, for which the ice-nucleating behaviour is well-characterised. In these experiments, $N_{INP}(T)$ is expected to increase sharply with decreasing temperature and then plateau [Wex et al., 2015]. If no ice crystals were lost in an expansion, this same increase should be observed at higher pressures, followed by a plateau in the lower pressure bins. However, in our PINE data, the $n_s(T)$ reaches a maximum at approximately 850 hPa and subsequently decreases slightly at lower pressures (Figure S14). This behaviour indicates that the ice crystal losses become significant below this pressure cutoff, rendering the data unreliable. Based on this consistent feature across the dry Snomax PINE experiments, we define 850 hPa as the minimum reliable pressure for all PINE experiments and exclude all pressure bins below this threshold in our analysis. This approach removes the low bias introduced by ice crystal loss. The dry Snomax PINE data with the 850 hPa pressure cutoff can be seen in Figure S14.

## References

O. Möhler, S. Benz, H. Saathoff, M. Schnaiter, R. Wagner, J. Schneider, S. Walter, V. Ebert, and S. Wagner. The effect of organic coating on the heterogeneous ice nucleation efficiency of mineral dust aerosols. *Environmental Research Letters*, 3(2), 6 2008. ISSN 17489326. doi: 10.1088/1748-9326/3/2/025007.

H. Wex, S. Augustin-Bauditz, Y. Boose, C. Budke, J. Curtius, K. Diehl, A. Dreyer, F. Frank, S. Hartmann, N. Hiranuma, E. Jantsch, Z. A. Kanji, A. Kiselev, T. Koop, O. Möhler, D. Niedermeier, B. Nillius, M. Rösch, D. Rose, C. Schmidt, I. Steinke, and F. Stratmann. Intercomparing different devices for the investigation of ice nucleating particles using Snomax® as test substance. *Atmospheric Chemistry and Physics*, 15(3):1463–1485, 2 2015. ISSN 16807324. doi: 10.5194/acp-15-1463-2015.